FINITE ELEMENT MODELING OF PIEZOELECTRIC STRUCTURES

Vincent PIEFORT & André PREUMONT
Active Structures Laboratory, ULB - CP 165/42
Av F.D. Roosevelt 50, B-1050 Brussels, Belgium

(eMail: Vincent.Piefort@ulb.ac.be, http://www.ulb.ac.be/scmero)

ABSTRACT:
The design of control systems involving piezoelectric actuators and sensors requires an accurate knowledge of the transfer functions between the inputs and the outputs of the system. These are not easy to determine numerically, particularly for shell structures with embedded distributed actuators and sensors. The situation where they are nearly collocated is particularly critical, because the zeros of the transfer functions are dominated by local effects which can only be accounted for by finite elements.
This paper presents a general finite element formulation for piezoelectrically coupled systems. Piezoelectric finite elements were developed based on Mindlin shell elements and integrated in the FE package Samcef. Volume elements have also been derived and integrated.
Volume finite element and shell finite element solutions are compared for the bimorph device. A shear actuation device is modelized. The interfacing with a control oriented software environment is discussed and non-trivial applications in noise and vibration control are presented.

1 PIEZOELECTRIC FINITE ELEMENTS

The constitutive equations of a linear piezoelectric material read (IEEE std, 1988).

$$\{T\} = [c^E]\{S\} - [e]^T\{E\} \quad (1)$$
$$\{D\} = [e]\{S\} + [\varepsilon^S]\{E\} \quad (2)$$

where $\{T\} = \{T_{11}\ T_{22}\ T_{33}\ T_{23}\ T_{13}\ T_{12}\}^T$ is the stress vector, $\{S\} = \{S_{11}\ S_{22}\ S_{33}\ 2S_{23}\ 2S_{13}\ 2S_{12}\}^T$ the deformation vector, $\{E\} = \{E_1\ E_2\ E_3\}$ the electric field, $\{D\} = \{D_1\ D_2\ D_3\}$ the electric displacement, $[c]$ the elasticity constants matrix, $[\varepsilon]$ the dielectric constants matrix, $[e]$ the piezoelectric coupling coefficients matrix (superscripts ^{E} and ^{S} indicate values at E and S constant respectively)

The dynamic equations of a piezoelectric continuum can be derived from the *Hamilton* principle, in which the Lagrangian and the virtual work are properly adapted to include the electrical contributions as well as the mechanical ones. The potential energy density of a piezoelectric material includes contributions from the strain energy and from the

electrostatic energy (Tiersten, 1967).

$$H = \frac{1}{2}\left[\{S\}^T\{T\} - \{E\}^T\{D\}\right] \tag{3}$$

Similarly, the virtual work density reads

$$\delta\mathcal{W} = \{\delta u\}^T\{F\} - \delta\phi\ \sigma \tag{4}$$

where $\{F\}$ is the external force and σ is the electric charge. From Equ.(3) and (4), the analogy between electrical and mechanical variables can be deduced (Table 1).

Mechanical		Electrical	
Force	$\{F\}$	σ	Charge
Displ.	$\{u\}$	ϕ	Voltage
Stress	$\{T\}$	$\{D\}$	Electric Displ.
Strain	$\{S\}$	$\{E\}$	Electric Field

Table 1: Electromechanical analogy

The variational principle governing the piezoelectric materials follows from the substitution of H and $\delta\mathcal{W}$ into the *Hamilton* principle (Allik and Hughes, 1970).

$$\begin{aligned} 0 \;=\; & -\int_V \Big[\rho\{\delta u\}^T\{\ddot{u}\} - \{\delta S\}^T[c^E]\{S\} + \{\delta S\}^T[e]^T\{E\} + \{\delta E\}^T[e]\{S\} \\ & + \{\delta E\}^T[\varepsilon^S]\{E\} + \{\delta u\}^T\{P_b\}\Big]\, dV + \int_{S_1}\{\delta u\}^T\{P_S\}dS \\ & + \{\delta u\}^T\{P_c\} - \int_{S_2}\delta\phi\ \sigma\ dS - \delta\phi\ Q \end{aligned} \tag{5}$$

In the finite element formulation, the displacement field $\{u\}$ and the electric potential ϕ over an element are related to the corresponding node values $\{u_i\}$ and $\{\phi_i\}$ by the mean of the shape functions $[\mathcal{N}_u]$, $[\mathcal{N}_\phi]$

$$\{u\} = [\mathcal{N}_u]\{u_i\} \tag{6}$$
$$\phi = [\mathcal{N}_\phi]\{\phi_i\} \tag{7}$$

And therefore, the strain field $\{S\}$ and the electric field $\{E\}$ are related to the nodal displacements and potential by the shape functions derivatives $[\mathcal{B}_u]$ and $[\mathcal{B}_\phi]$ defined by

$$\{S\} = [\mathcal{D}][\mathcal{N}_u]\{u_i\} = [\mathcal{B}_u]\{u_i\} \tag{8}$$
$$\{E\} = -\nabla[\mathcal{N}_\phi]\{\phi_i\} = -[\mathcal{B}_\phi]\{\phi_i\} \tag{9}$$

where ∇ is the gradient operator and $[\mathcal{D}]$ is the derivation operator defined such as $\{S\} = [\mathcal{D}]\{u\}$.

Substituting expressions (6) to (9) into the variational principle (5) yields

$$
\begin{aligned}
0 = & - \{\delta u_i\}^T \int_V \rho [\mathcal{N}_u]^T [\mathcal{N}_u] dV \{\ddot{u}_i\} - \{\delta u_i\}^T \int_V [\mathcal{B}_u]^T [c^E] [\mathcal{B}_u] dV \{u_i\} \\
& - \{\delta u_i\}^T \int_V [\mathcal{B}_u]^T [e] [\mathcal{B}_\phi] dV \{\phi_i\} - \{\delta \phi_i\}^T \int_V [\mathcal{B}_\phi]^T [e]^T [\mathcal{B}_u] dV \{u_i\} \\
& + \{\delta \phi_i\}^T \int_V [\mathcal{B}_\phi]^T [\varepsilon^S] [\mathcal{B}_\phi] dV \{\phi_i\} + \{\delta u_i\}^T \int_V [\mathcal{N}_u]^T \{P_b\} dV \\
& + \{\delta u_i\}^T \int_{S_1} [\mathcal{N}_u]^T \{P_S\} dS + \{\delta u_i\}^T [\mathcal{N}_u]^T \{P_c\} \\
& - \{\delta \phi_i\}^T \int_{S_2} [\mathcal{N}_\phi]^T \sigma dS - \{\delta \phi_i\}^T [\mathcal{N}_\phi]^T Q
\end{aligned} \tag{10}
$$

which must be verified for any arbitrary variation of the displacements $\{\delta u_i\}$ and electrical potentials $\{\delta \phi_i\}$ compatible with the *essential* boundary conditions.

For an element, Equ.(10) can be written under the form

$$
[\mathcal{M}]\{\ddot{u}_i\} + [K_{uu}]\{u_i\} + [K_{u\phi}]\{\phi_i\} = \{f_i\} \tag{11}
$$

$$
[K_{\phi u}]\{u_i\} + [K_{\phi\phi}]\{\phi_i\} = \{g_i\} \tag{12}
$$

with

$$
[\mathcal{M}] = \int_V \rho [\mathcal{N}_u]^T [\mathcal{N}_u] dV \tag{13}
$$

$$
[K_{uu}] = \int_V [\mathcal{B}_u]^T [c^E] [\mathcal{B}_u] dV \tag{14}
$$

$$
[K_{u\phi}] = \int_V [\mathcal{B}_u]^T [e]^T [\mathcal{B}_\phi] dV \tag{15}
$$

$$
[K_{\phi\phi}] = - \int_V [\mathcal{B}_\phi]^T [\varepsilon] [\mathcal{B}_\phi] dV \tag{16}
$$

$$
[K_{\phi u}] = [K_{u\phi}]^T \tag{17}
$$

respectively the element mass, stiffness, piezoelectric coupling and capacitance matrix and

$$
\{f_i\} = \int_V [\mathcal{N}_u]^T \{P_b\} dV + \int_{S_1} [\mathcal{N}_u]^T \{P_S\} dS + [\mathcal{N}_u]^T \{P_c\} \tag{18}
$$

$$
\{g_i\} = - \int_{S_2} [\mathcal{N}_\phi]^T \sigma dS - [\mathcal{N}_\phi]^T Q \tag{19}
$$

the external mechanical force and electric charge.

Each element k of the mesh is connected to its neighbouring elements at the global nodes and the displacement is continuous from one element to the next.

Based on that formulation, piezoelectric finite elements of type multilayered *Mindlin* shell (Piefort and Preumont, 2000) and volume have been derived.

For shell elements, it is assumed that the electric field and displacement are uniform across the thickness and aligned on the normal to the mid-plane. The electrical degrees of freedom are the voltages ϕ_k across the piezoelectric layers; it is assumed that the voltage is

constant over each element (this implies that the finite element mesh follows the shape of the electrodes). One electrical *degree of freedom* of type *voltage* per piezoelectric layer is defined. The assembly takes into account the equipotentiality condition of the electrodes; this reduces the number of electric variables to the number of electrodes.

For volume elements, one additional *degree of freedom* of type *electric potential* is defined in each node of the piezoelectric volume element.

2 STATE SPACE MODEL

The idea behind modelling structures embedding piezoelectric actuators and sensors using finite elements is indeed to gather the necessary informations to design a good control strategy. It is therefore necessary to interface the structural analysis software (finite element package) with a control design software.

The assembled system of equations can be complemented with a damping term $[C]\{\dot{U}\}$ to obtain the full equation of dynamics and the sensor equation:

$$\begin{aligned} \{0\} &= [\mathcal{M}]\{\ddot{U}\} + [C]\{\dot{U}\} \\ &\quad +[K_{UU}]\{U\} + [K_{U\Phi}]\{\Phi\} \qquad (20) \\ \{G\} &= [K_{\Phi U}]\{U\} + [K_{\Phi\Phi}]\{\Phi\} \qquad (21) \end{aligned}$$

where $\{U\}$ represents the mechanical *dof*, $\{\Phi\}$ the electric potential *dof*, $[\mathcal{M}]$ the inertial matrix, $[C]$ the damping matrix, $[K_{UU}]$ the mechanical stiffness matrix, $[K_{U\Phi}] = [K_{\Phi U}]^T$ the electromechanical coupling matrix and $[K_{\Phi\Phi}]$ the electric capacitance matrix.

Voltage actuation and charge sensing are considered. Actuation is done by imposing a voltage $\{\Phi\}$ on the actuators and sensing by imposing a zero voltage ($\{\Phi\} = \{0\}$) and measuring the electric charges $\{G\}$ appearing on the sensors.

Using a truncated modal decomposition (n decoupled modes) $\{U\} = [\mathcal{Z}]\{x(t)\}$, where $[\mathcal{Z}]$ represents the n modal shapes and $\{x(t)\}$ the n modal amplitudes, Equ.(20) and (21) become

$$\begin{aligned} \{0\} &= [\mathcal{M}][\mathcal{Z}]\{\ddot{x}\} + [C][\mathcal{Z}]\{\dot{x}\} + [K_{UU}][\mathcal{Z}]\{x\} + [K_{U\Phi}^{(i)}]\{\Phi\} \qquad (22) \\ \{G\} &= [K_{\Phi U}^{(o)}][\mathcal{Z}]\{x\} + [K_{\Phi\Phi}]\{\Phi\} \qquad (23) \end{aligned}$$

and left-multiplying Equ.(22) by $[\mathcal{Z}]^T$ using the orthogonality properties of the mode shapes.

$$\begin{aligned} [\mathcal{Z}]^T [\mathcal{M}] [\mathcal{Z}] &= \mathrm{diag}(\mu_k) \qquad (24) \\ [\mathcal{Z}]^T [K] [\mathcal{Z}] &= \mathrm{diag}(\mu_k \omega_k^2) \qquad (25) \end{aligned}$$

and a classical damping

$$[\mathcal{Z}]^T [C] [\mathcal{Z}] = \mathrm{diag}(2\xi_k \mu_k \omega_k) \qquad (26)$$

the dynamic equations of the system in the state space representation finally read:

$$\left\{ \begin{array}{c} \dot{x} \\ \ddot{x} \end{array} \right\} = \left[\begin{array}{cc} 0 & I \\ -\Omega^2 & -2\xi\Omega \end{array} \right] \left\{ \begin{array}{c} x \\ \dot{x} \end{array} \right\} - \left[\begin{array}{c} 0 \\ \mu^{-1} \mathcal{Z}^T K_{U\Phi}^{(i)} \end{array} \right] \{\Phi\} \tag{27}$$

$$\{G\} = \left[\begin{array}{cc} {K_{U\Phi}^{(o)}}^T \mathcal{Z} & 0 \end{array} \right] \left\{ \begin{array}{c} x \\ \dot{x} \end{array} \right\} + [D_{HF}]\{\Phi\} \tag{28}$$

where the modal shapes $[\mathcal{Z}]$, the modal frequencies $[\Omega] = \mathrm{diag}(\omega_k)$, the modal masses $[\mu] = \mathrm{diag}(\mu_k)$, the modal electric charge on the sensor $[K_{\Phi U}^{(o)}][\mathcal{Z}]$, and the modal electric charge on the actuators, transposed (by reciprocity) $[\mathcal{Z}]^T[K_{U\Phi}^{(i)}]$, representing the participation factor of the actuators to each mode, are obtained from a *dynamic* finite element analysis.

$[\xi] = \mathrm{diag}(\xi_k)$ are the modal classical damping ratios of the considered structure and $[D_{HF}]$ is the static contribution of the high frequency modes (Preumont, 1997; Loix, 1998; Loix et al., 1998); Its elements are given by

$$D_{lm} = d_{lm} - \sum_{k=1}^{n} \frac{(K_{\Phi U}^{(o)} \mathcal{Z}_k)_l (\mathcal{Z}_k^T K_{U\Phi}^{(i)})_m}{\mu_k \omega_k^2} \tag{29}$$

where d_{lm} is the charge appearing on the l^{th} sensor when a unit voltage is applied on the m^{th} actuator and is obtained from a *static* finite element analysis.

Such a state space representation is easily implemented in a control oriented software allowing the designer to extract the various transfer functions and use the control design tools.

3 APPLICATIONS

3.1 Bimorph beam

The piezoelectric bimorph pointer (Fig.1) is a beam made of two uniaxial piezoelectric layers with opposite polarities stacked together to obtain a bending actuator/sensor. This device can be used for micro-actuation or strain sensing.

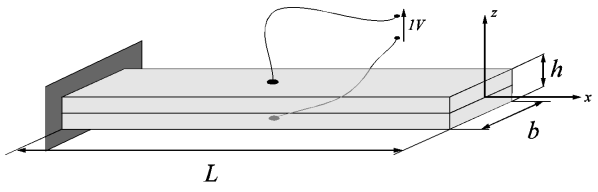

Figure 1: Bimorph pointer

When an external voltage is applied accross the thickness, the induced strain generates moments that bend the bimorph beam.

Conversely, the piezoelectric bimorph beam can also be used for sensing: a tip deflection of 10 mm is imposed and the output voltage accross the thickness is calculated (voltage between electrodes, the circuit being left open). The considered sensor electrodes configuration consists in five identical pairs of electrodes distributed along the length (Fig.2).

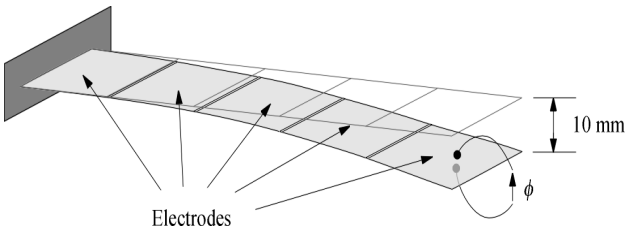

Figure 2: Bimorph sensor

The result given by a 50 volume elements mesh is compared to the 5 shell elements mesh result on Fig.3.

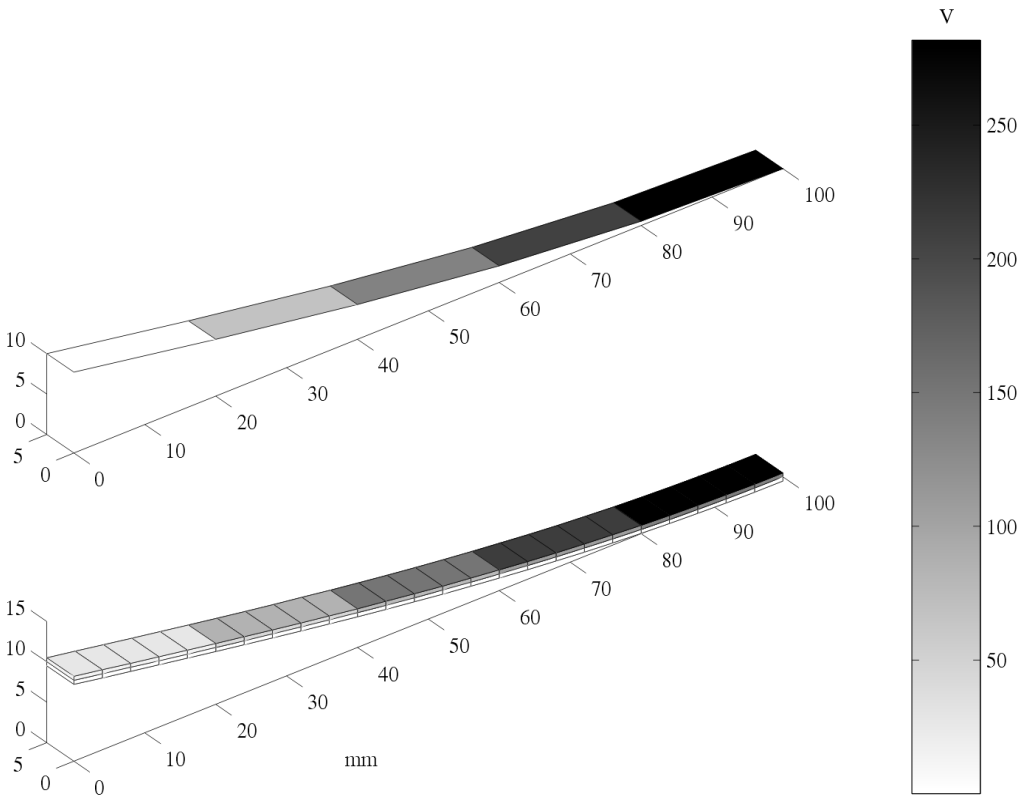

Figure 3: Shells - Volumes comparison

3.2 Shear actuator

The use of the shear mode of piezoelectric materials has been investigated in (Benjeddou et al., 1998). The proposed architecture consists in a sandwiched beam for which part of the core has been replaced by piezoelectric material. The proposed configuration is such that, this time, the d_{15} coupling coefficient dictates the design. The electric field is applied perpendicularly to the poling direction, inducing a transverse shear strain. A finite element solution using sandwich beam has been proposed by Benjeddou et al. and compared to analytical results. The bender of Fig.4 is considered.

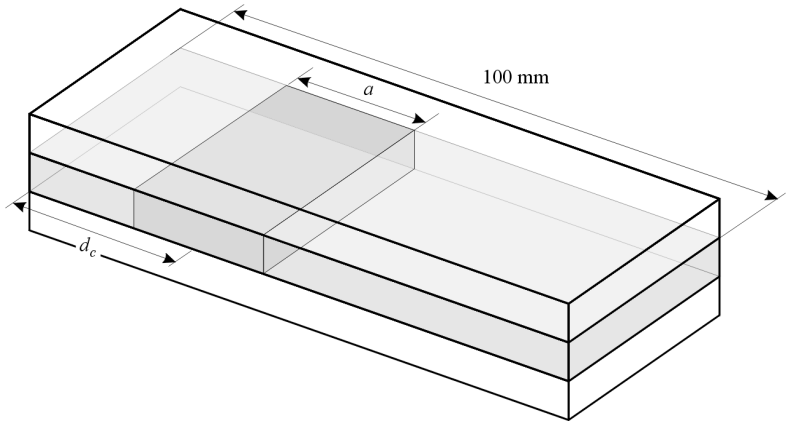

Figure 4: Shear bender

It consists in a cantilever beam 100 mm long formed of a 2 mm rigid foam core sandwiched by two 8 mm thick aluminium skins. The core is partially replaced by *PZT* piezoceramics to form an actuator of length a at a distance d_c from the clamp. A 20 V voltage is applied between top and bottom surfaces of the piezoelectric layer. The material properties are summarized in table 2.

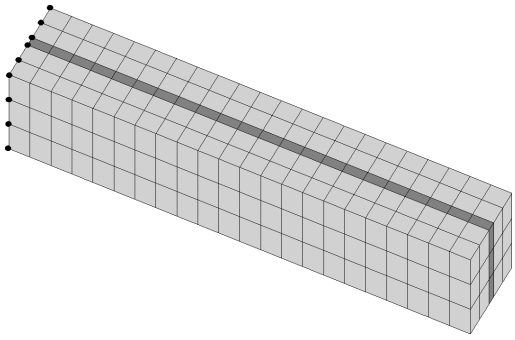

Figure 5: FE mesh

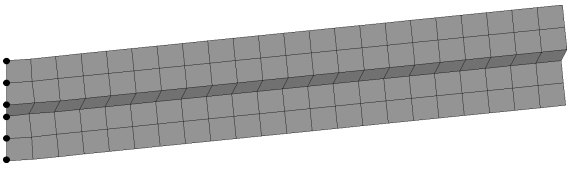

Figure 6: Static deformation

As a first test case, the core is totally replaced by the piezoactuator (there is no rigid foam). The mesh is shown on Fig. 5 and the static deformation on Fig.6. The comparison with the FE and analytical results from (Benjeddou et al., 1998) shows a good agreement.

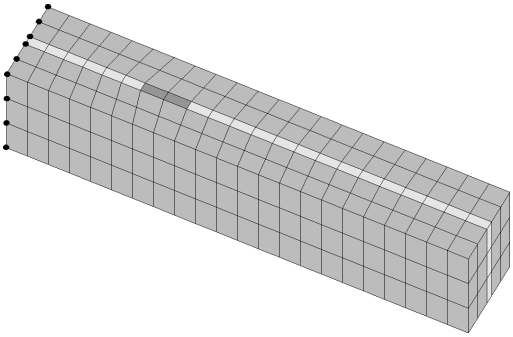

Figure 7: FE mesh

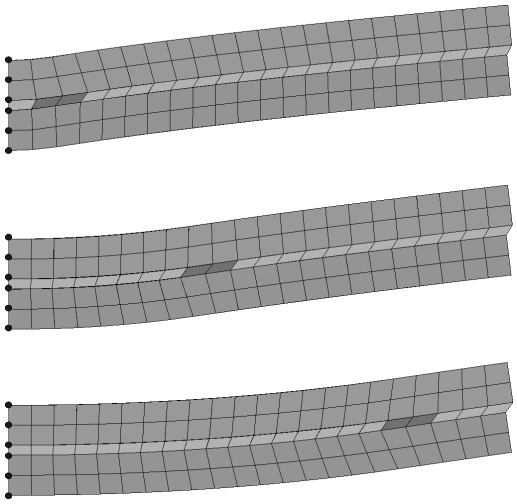

Figure 8: Resulting deformation

As a second case, an actuator of length $a = 10$ mm replace part of the core. Its position is set to vary between 10 mm and 90 mm. The mesh is shown on Fig. 7 and resulting deformations for different locations of the actuator are shown on Fig.8.

Aluminium		
ρ	2690	kg/m^3
Y	70.3	GPa
ν	0.345	
Foam		
ρ	2690	kg/m^3
Y	70.3	GPa
ν	0.345	
PZT-5H		
ρ	7730	kg/m^3
$[c]$	$\begin{bmatrix} 126 & 79.5 & 84.1 & 0 & 0 & 0 \\ 79.5 & 126 & 84.1 & 0 & 0 & 0 \\ 84.1 & 84.1 & 126 & 0 & 0 & 0 \\ 0 & 0 & 0 & 23.3 & 0 & 0 \\ 0 & 0 & 0 & 0 & 23.0 & 0 \\ 0 & 0 & 0 & 0 & 0 & 23.0 \end{bmatrix}$	GPa
$[\varepsilon]$	$\begin{bmatrix} 1.503 & 0 & 0 \\ 0 & 1.503 & 0 \\ 0 & 0 & 1.3 \end{bmatrix} 10^{-8}$	F/m
$[e]$	$\begin{bmatrix} 0 & 0 & 0 & 0 & 0 & 17 \\ 0 & 0 & 0 & 0 & 17 & 0 \\ -6.5 & -6.5 & 23.3 & 0 & 0 & 0 \end{bmatrix}$	Cb/m

Table 2: Material properties

3.3 Volume velocity control: ASAC

At low frequency, there is a strong correlation between the sound power radiated by a baffled plate and its volume velocity. The *ASAC* panel (Active Structural Acoustical Control) (Gardonio et al., 1999) is a volume velocity control device based on the same principle as the *QWSIS* sensor (Quadratically Weighted Strain Integration Sensor) (Rex and Elliott, 1992) for both actuation and sensing. It consists in a clamped plate of aluminium covered on both side with piezoelectric *PVDF* film. It exhibits a pair of colocated quadratically shaped actuator/sensor.

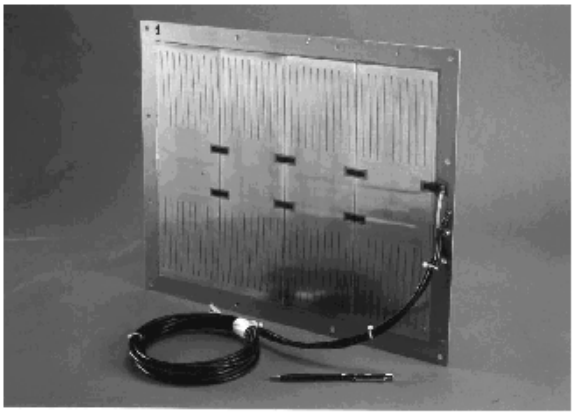

Figure 9: *ASAC* experimental setup

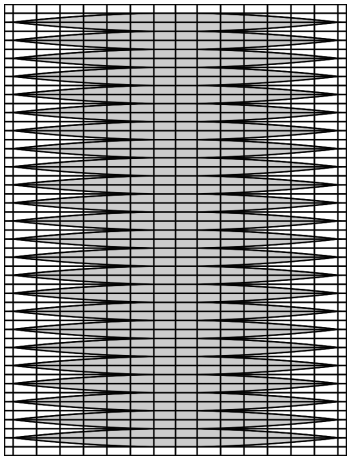

Figure 10: *FE* mesh

It consists in a clamped 1 mm thick plate of aluminium (420 mm$\times 320$ mm) covered on both side with 0.5 mm thick piezoelectric *PVDF* film (400 mm$\times 300$ mm). The electrodes of both layers are milled in a quadratic shape. This electrodes shaping provides an inherent spatial integration giving an input load equivalent to a uniform pressure and an output signal proportional to the volume velocity.

Aluminium		
Y	71	(GPa)
ν	0.3	
ρ	2800	(kg/m^3)
PVDF		
Y	2.7	(GPa)
ν	0.29	
ρ	1800	(kg/m^3)
d_{31}	1.8 10^{-11}	(Cb/N)
d_{32}	0.3 10^{-11}	(Cb/N)
ε_r	2600	

Table 3: Material properties

For the actual laboratory model (*ISVR*) the actuation and sensing layers electrodes present 24 strips. The material properties are summarized in table 3. The direction of smaller piezoelectric coupling coefficient (d_{32}) is perpendicular to the strips. The experimental setup is sketched on fig.9. The finite element mesh used is shown on fig.10.

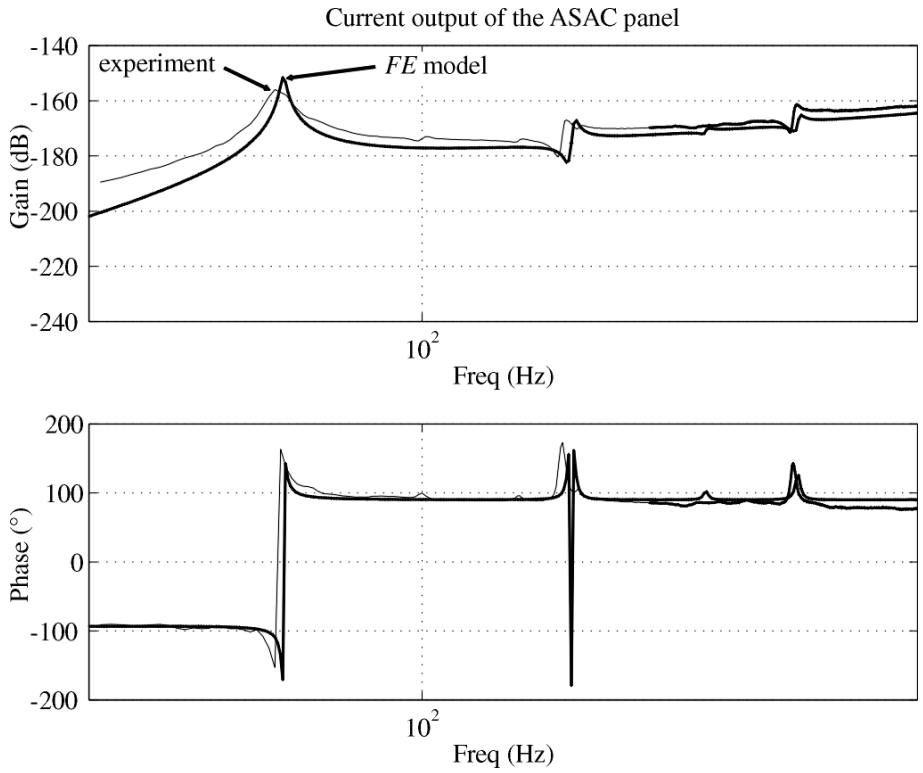

Figure 11: Open loop transfer functions

The foreseen explanation for the rather poor controllability of the actual experimental setup compared to the expectations was that the top and bottom layers were not perfectly aligned and therefore did not form a colocated actuator/sensor pair.

The finite element simulations have shown that this lack of controllability is actually due to local membrane effects (Piefort and Henrioulle, 2000), neglected in the first analytical models together with the static contribution of the non-modelized high frequency modes.

The in-plane movement of the plate (not fixed in the actual experiment) results in a stronger influence of the membrane component and, therefore, in a stronger in-plane mechanical coupling between actuator and sensor. This induces an important feedthrough term in the transfer function. The results of the *FE* simulation are shown on Fig.11; they show a very good agreement with the experiments.

This test case illustrates the situation of shell structures with embedded piezoelectric actuators and sensors where they are nearly collocated. It stresses the importance of membrane components on the zeros of the transfer function. These local effects can easily be accounted for by the developped modelling tools based on finite elements.

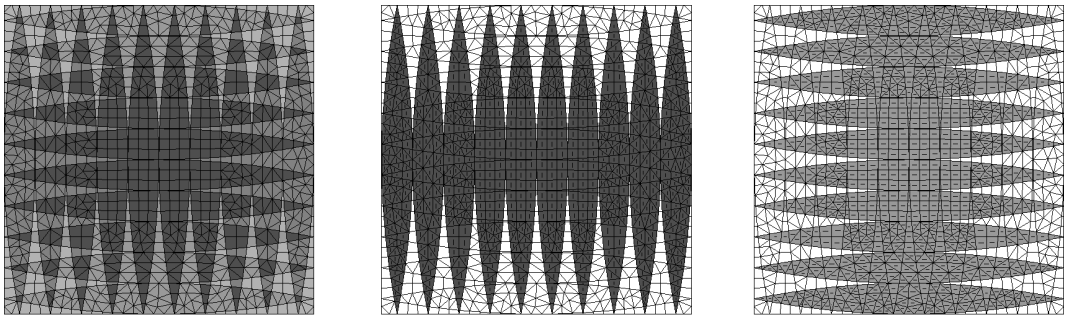

Figure 12: FE mesh

As the piezoelectric coupling characteristics of the considered *PVDF* and the electrodes shape are highly unidirectional, the idea raised of using sensor strips perpendicular to the actuator strips. The control device would then exhibit a *cross-ply* actuator/sensor architecture and the in-plane feedthrough term would be greatly reduced. The *FE*-based tools allow to modelize such architectures quite easily and to extract the corresponding transfer functions to verify if this alternative is any better.

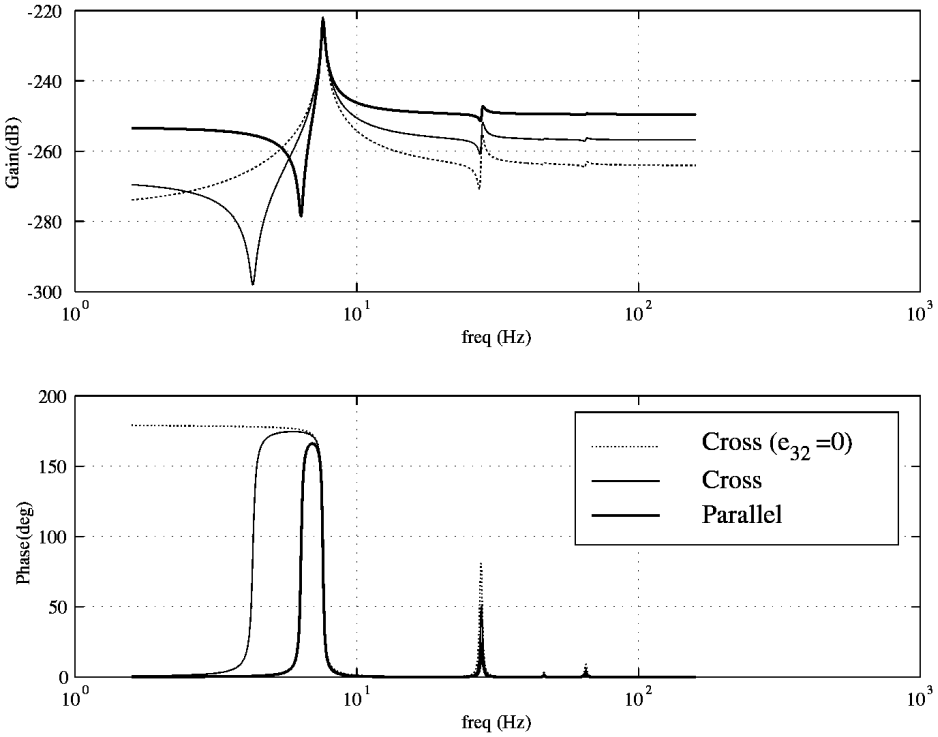

Figure 13: Open loop transfer functions

The mesh used is represented on Fig.12; the sensor electrode forms a right angle with the actuator electrode. The comparison of the transfer functions between the voltage applied

to the actuator layer and the charge measured on the sensor layer for the *parallel* and *cross-ply* architectures are represented on Fig.13.

The open loop transfer function of the *cross-ply* architecture system shows a bigger distance between poles and zeros. A better controllability can therefore be expected (See Preumont, 1997).

3.4 Noise radiation sensor: ALC

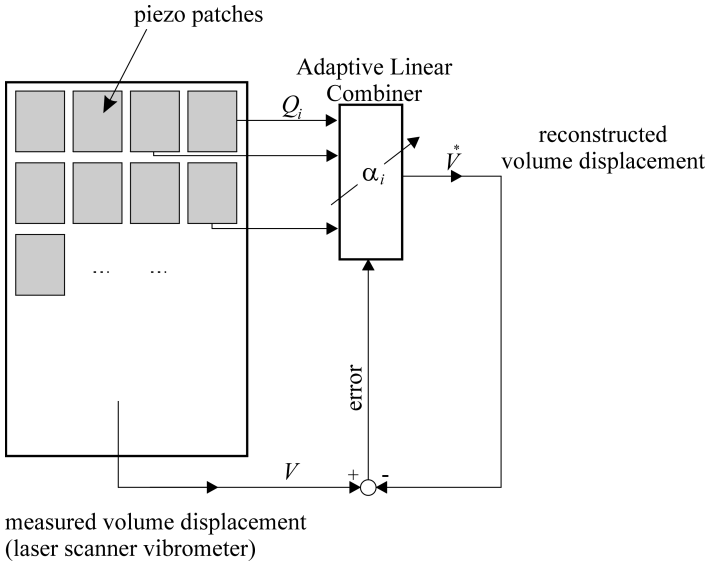

Figure 14: Principle of the volume displacement sensor

A noise radiation sensor consisting of an array of independent piezoelectric patches connected to an adaptive linear combiner was proposed (Preumont et al., 1999). The coefficients of the linear combiner are adapted in such a way that the mean-square error between the reconstructed volume displacement (or velocity) and either numerical or experimental data is minimized.

More precisely, this sound radiation sensor consists of an array of piezoelectric patches located at the nodes of a rectangular mesh; the electric charges Q_i induced on the various patches by the plate vibration are the independent inputs of a multiple input adaptive linear combiner (Fig.14).

This strategy can be used for reconstructing the volume displacement of a baffled plate with arbitrary boundary conditions. If the piezoelectric patches are connected to current amplifiers instead of charge amplifiers, the output signal becomes the volume velocity instead of the volume displacement.

The laboratory demonstration model shown on Fig.15 consists in a simply supported glass plate (54 cm $\times$ 124 cm, 4 mm thick) covered with an array of 4 by 8 piezoelectric patches

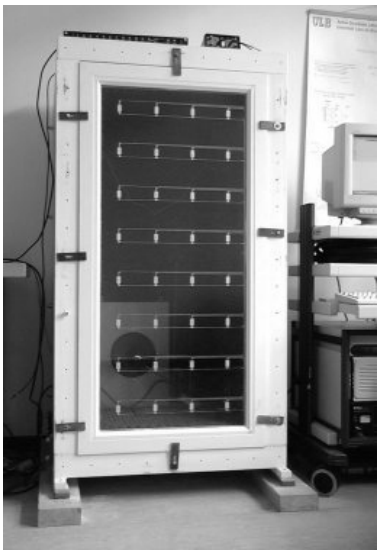

Figure 15: Experimental setup

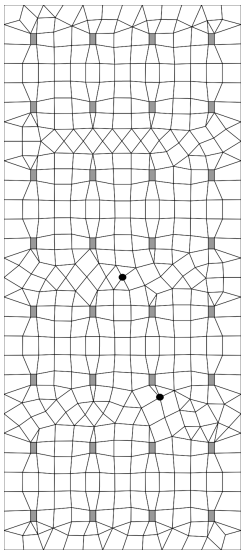

Figure 16: *FE* mesh

St-Roch Glass		
Y	72	(GPa)
ν	0.22	
ρ	2500	(kg/m^3)
PZT		
Y	69	(GPa)
ν	0.3	
ρ	7800	(kg/m^3)
d_{31}	205 10^{-12}	(Cb/N)
d_{32}	205 10^{-12}	(Cb/N)
ε_r	2600	

Table 4: Material properties

(*PZT* - 13.75 mm $\times$ 25 mm, 0.25 mm thick). The materials properties are summarized in Table 4.

We used the opportunity given by the scanner laser interferometer to measure the velocity of an array of points over the window to deduce the volume velocity. The excitation used was provided by two shakers actuating the window directly.

The finite element mesh used for the numerical analysis is represented on fig.16. The 30 first vibration modes were taken into account for the dynamic analysis. Figure 17 shows the comparison between the transfer functions between the excitation of Shaker #1 (in the center of the window) and, respectively, sensors 7, 14 and the volume velocity obtained by finite element analysis and experimentally.

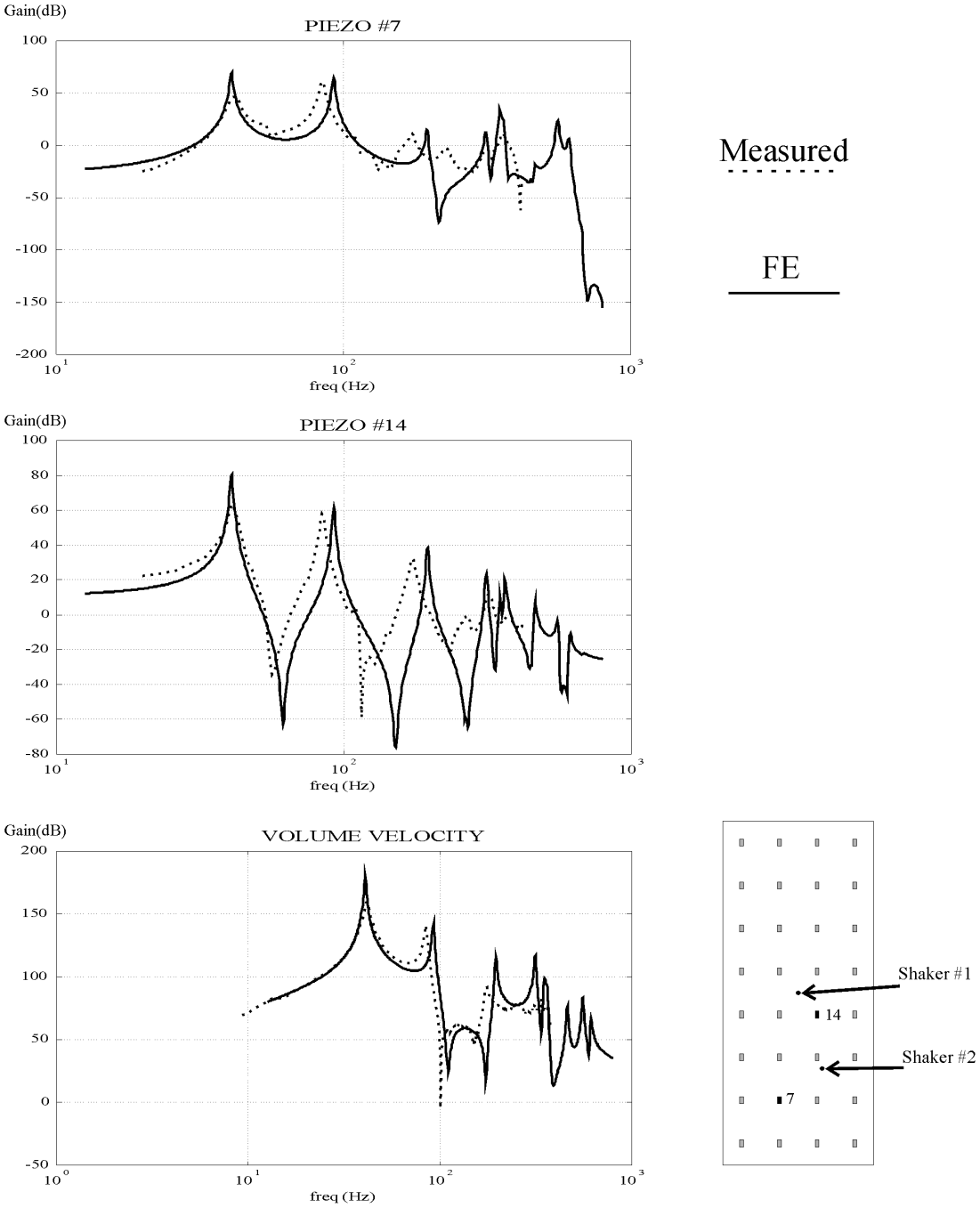

Figure 17: Transfer Functions /Shaker #1

3.5 Design against fatigue

Fatigue damage is one of the most frequent form of failure of metallic structures. With the increasing demand for high performance structures, the fatigue damage has become more and more important, in particular for metallic structures subjected to complex multiaxial

loads due to random vibrations.

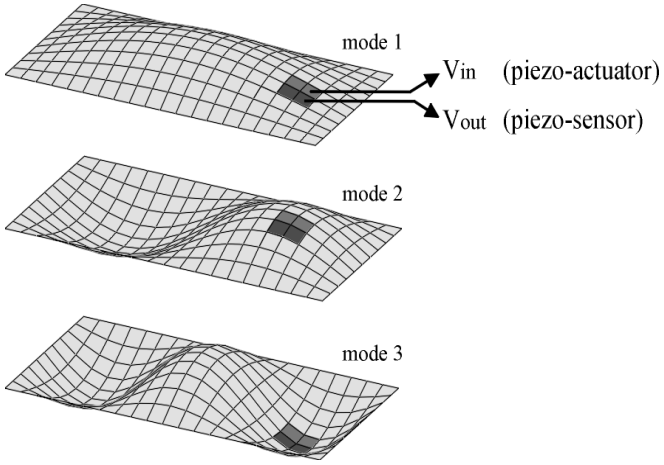

Figure 18: Piezoelectric elements location and first vibration modes

The active damping can be considered as a solution to reduce the vibrations level and at the same time, reduce the weight and increase the fatigue lifetime of such structures. Simulation tools allowing the designer to include directly piezoelectric actuators and sensors in a finite-element model have been developed as well as a *multiaxial random fatigue matlab toolbox* (Pitoiset et al., 1998; Pitoiset and Preumont, 2000) allowing the direct assessment of the fatigue lifetime of a structure from a spectral analysis.

The quantification of the damage reduction that can be achieved thanks to an active damping can then be performed very easily, directly from a modal and a spectral analysis with finite-elements. This has been done on a simple example: A simply supported rectangular steel plate (15.24 cm$\times 30.48$ cm$\times 0.813$ mm) is considered.

It is subjected to a band limited white noise random pressure field with perfect spatial coherence; Its *PSD* (Power Spectral Density) is the following: $\Phi_{pp}(\omega) = 400$ Pa^2/rad/s between 0 Hz and 1000 Hz. The first three vibration modes are within the bandwidth of excitation. A piezoelectric actuator and a piezoelectric sensor (*PZT* 15.24 cm$\times 30.48$ mm$\times 0.2$ mm) are bonded to the surface as shown on fig.18.

The *multiaxial random fatigue matlab toolbox* was used after a *FE* spectral analysis to evaluate the fatigue damage ratio (per second) over the plate. The state space form of the system is built under *MATLAB* directly from the results of a *FE* modal analysis. A controller is designed using *MATLAB* functionalities, in this case: a *PPF* tuned on the first mode (Positive Position Feedback).

The new modal damping ratios and eigen frequencies can be used in the *multiaxial random fatigue matlab toolbox* to evaluate the fatigue damage ratio over the controlled plate. The comparison between damage maps for the plate without and with active damping is shown on fig.19.

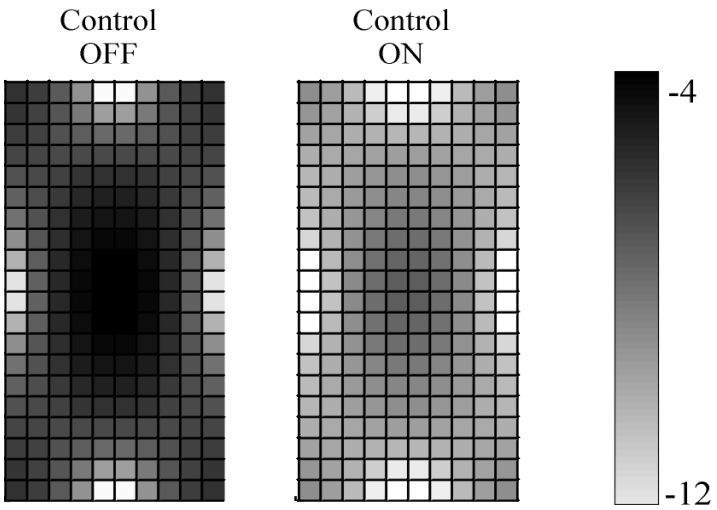

Figure 19: Damage map (Von Mises) with and without control (Log Scale)

4 CONCLUSIONS

A finite element formulation for an electromechanically coupled piezoelectric structure starting from the constitutive equations has been presented. General multilayered piezoelectric shell elements have been succesfully developed and integrated into the commercial finite element package *Samcef*. Volume elements have also been implemented. A method to extract a state space model of a piezoelectric input/output system from the modal finite element analysis of the structure has been presented.

Applications of the developped tools in structure embedded actuation and sensing and in vibration and vibroacoustic control have been described and show that good performances can be achieved. The importance of the in-plane components in the open loop transfer functions has been stressed.

An application consisting in the design of an active damping system to increase the fatigue lifetime of a metallic structure submitted to random vibrations and illustrates some possibilities of the developped tools.

5 ACKNOWLEDGEMENT

This study has been supported by a research grant from the *Région Wallonne, Direction Générale des Technologies, de la Recherche et de l'Energie*; The support of the IUAP-4/24 on *Intelligent Mechatronic Systems* (Belgian programme on Interuniversity Poles of Attraction initiated by the Belgian State, Prime Minister's Office, Science Policy Programming) is also acknowledged. The technical assistance of *Samtech s.a.* is deeply appreciated.

REFERENCES

Allik, H. and T. J. R. Hughes, 1970, “Finite Element Method for Piezoelectric Vibration”, *International Journal for Numerical Methods in Engineering*, 2:151–157.

Benjeddou, A., M. A. Trindade, and R. Ohayon, 1998, “A new shear actuated smart structure beam element”, AIAA 98-1922.

Gardonio, P., et al., 1999, “Active Control of Sound Transmission Through a Panel with a Matched PVDF Sensor and Actuator Pair”, Active 99, Fort Lauderdale, Florida, USA.

IEEE std, 1988, “IEEE Standard on Piezoelectricity – ANSI/IEEE Std 176-1987”, .

Loix, N., 1998, *Amortissement Actif de Structures Flexibles*, Ph.D. thesis, Université Libre de Bruxelles - Faculté des Sciences Appliquées.

Loix, N., V. Piefort, and A. Preumont, 1998, “Modeling aspects of active structures with collocated piezoelectric actuators and sensors”, *Benelux Quarterly Journal on Automatic Control (Journal $\mathcal{A}$)*, 39(1).

Piefort, V. and K. Henrioulle, 2000, “Modelling of Smart Structures with Colocated Piezoelectric Actuator/Sensor Pairs: Influence of the in-Plane Components”, Fifth International Conference on Computational Structures Technology, Leuven, Belgium.

Piefort, V. and A. Preumont, 2000, “Modeling of Smart Piezoelectric Structures with Finite Elements”, ISMA25, 25th International Conference on Noise and Vibration Engineering, Leuven, Belgium.

Pitoiset, X. and A. Preumont, 2000, “Spectral Methods for Multiaxial Random Fatigue Analysis of Metallic Structures”, *International Journal of Fatigue*, 22(7):541–550.

Pitoiset, X., A. Preumont, and A. Kernilis, 1998, “Tools for a multiaxial fatigue analysis of structures submitted to random vibration”, European Conference on Spacecraft Structures, Materials and Mechanical Testing, Braunschweig.

Preumont, A., 1997, *Vibration Control of Active Structures - An Introduction*, Kluwer Academic Publishers.

Preumont, A., A. François, and S. Dubru, 1999, “Piezoelectric Array Sensing for Real-Time, Broad-Band Sound Radiation Measurement”, *Journal of Vibration and Acoustics*, 121.

Rex, J. and S. J. Elliott, 1992, “The QWSIS - A New Sensor for Structural Radiation Control”, MOVIC-1, Yokohama.

Tiersten, H. F., 1967, “Hamilton’s Principle For Linear Piezoelectric Media”, in “Proceedings of the IEEE”, pages 1523–1524.